Original Article

Reproducibility of functional lung parameters derived from free-breathing non-contrast-enhanced 2D ultrashort echo-time

Bingjie Yang[1]^, Patrick Metze[1], Anke Balasch[1], Kilian Stumpf[1], Meinrad Beer[2], Wolfgang Rottbauer[1], Volker Rasche[1]

[1]Department of Internal Medicine II, Ulm University Medical Centre, Ulm, Germany; [2]Department of Radiology, Ulm University Medical Centre, Ulm, Germany

Contributions: (I) Conception and design: V Rasche, W Rottbauer, M Beer, B Yang; (II) Administrative support: V Rasche, W Rottbauer, M Beer; (III) Provision of study materials or patients: V Rasche, W Rottbauer, M Beer; (IV) Collection and assembly of data: B Yang, A Balasch, P Metze, V Rasche; (V) Data analysis and interpretation: B Yang, A Balasch, V Rasche; (VI) Manuscript writing: All authors; (VII) Final approval of manuscript: All authors.

Correspondence to: Prof. Dr. Volker Rasche. Internal Medicine II, Ulm University Medical Centre, Albert-Einstein-Allee 23, 89081 Ulm, Germany. Email: volker.rasche@uni-ulm.de.

Background: Imaging the lung parenchyma with magnetic resonance imaging (MRI) is challenging due to cardiac and respiratory motion, the low proton density and short T_2* relaxation time, and therefore not well established in the clinical routine. As a further step in facilitating lung MRI for longitudinal monitoring, this study aimed to assess the reproducibility of 2D ultrashort echo time (UTE)-derived lung function parameters in healthy subjects.

Methods: In this study, a 2D UTE technique was combined with tiny golden angle (tyGA) ordering. Data were acquired either during breath-holds (BH) or continuously during free-breathing (FB) at a field strength of 3T. Retrospective self-gating (image- and k-space-based) was used to reconstruct respiratory and cardiac multistage images from the FB acquisitions. The reproducibility of functional lung parameters derived from BH and FB acquisitions was assessed for three independent examinations (M1–3). M1 and M2 were acquired within 2 h, whereas M3 was acquired at least 14 d after M1/2. Different respiratory and cardiac phases were reconstructed for three coronal slices. Quantitative analysis including proton fraction (f_P), apparent signal-to-noise ratio (apparent SNR), fractional ventilation (FV), and perfusion (f) was performed by two independent observers, and inter-measurement and inter-observer repeatability were assessed.

Results: All scans could be performed successfully in all volunteers. Intraclass correlation coefficients (ICC) of inter-measurement and inter-observer variability, and Bland-Altman analysis showed good to very good reproducibility. Larger breathing amplitudes were observed in the BH acquisitions, which also showed lower reproducibility when compared with the FB acquisitions. For the FB approach, the ICC ranged between 0.70 and 0.98 for all measurements, and ranged between 0.86 and 0.97 for the two observers. No bias or significant differences were observed between the three measurements or the two observers in healthy volunteers.

Conclusions: The study proves the feasibility of FB 2D tyGA UTE for lung imaging. Functional parameters derived from FB acquisitions are reproducible in healthy volunteers, allowing for further investigation of this technique in patients with various underlying diseases.

Keywords: Ultrashort echo-time (UTE); fractional ventilation (FV); lung density; perfusion; self-gating

Submitted Jan 29, 2022. Accepted for publication Jun 30, 2022.
doi: 10.21037/qims-22-92
View this article at: https://dx.doi.org/10.21037/qims-22-92

^ ORCID: 0000-0002-5809-2521.

Introduction

Magnetic resonance imaging (MRI) of the lung is challenging due to respiratory and cardiac motion, low proton density and multiple air-tissue interfaces causing a short T2* (1-3). Techniques enabling short echo-times (TE) and thereby allowing the imaging of tissues with short T2* like ultrashort echo time (UTE) and zero echo-time (ZTE) imaging have recently gained clinical attention (1,2,4-15). The radial center-out k-space filling ensures TE only limited by the time required for switching between transmit and receive state and shows excellent motion artifact properties in case of residual motion (16,17). Intrinsic sampling of the k-space center with each acquisition provides direct current (DC) gating information without additional measurements, making the UTE sequence suitable for self-gating. However, radial trajectories can be limited by the choice of angular increment between subsequent readouts. In certain cases (e.g., respiratory frequency similar to "rotational" frequency of the gradient) a non-ideal angular increment results in an uneven coverage of k-space after self-gating, which in turn leads to distinct streaking artifacts. One possibility to achieve uniform k-space coverage after gating is the use of tiny golden angle (tyGA) angular increments (18,19), facilitating nearly uniform angular distribution of readouts for almost any number of readouts and thus reducing streak artifacts, as well as allowing the reconstruction of real-time data at different temporal resolutions.

Contrast agents, hyperpolarized gases and pure oxygen have been applied to assess functional pulmonary parameters, such as ventilation and perfusion. However, related high costs, limited resources and complex administration have limited especially the use of hyperpolarized gases (e.g., ^{3}He, ^{129}Xe) or pure oxygen to a few sites (20,21).

As alternative, the analysis of intensity changes of the lung parenchyma over the respiratory and cardiac cycle has been reported to provide diagnostic lung function information without the need for any injected or inhaled contrast agent. Breath-hold (BH) acquisitions in end-inspiration (IN) and end-expiration (EX) have been shown to provide functional information of the lung by analysis of the respective intensity changes (22,23), but do rely on patient cooperation and reproducible respiratory amplitudes during the BH. Realtime MRI with subsequent Fourier analysis (FD) has been introduced for evaluation of lung ventilation and perfusion by spectral analysis of intensity changes of the parenchyma during free breathing (24,25). This rather qualitative assessment of lung ventilation and perfusion was extended to provide quantitative perfusion data by analysis of signal intensity differences between blood-filled volumes and lung parenchyma (26). Even though applied to different pathologies and shown to provide reproducible information (27,28), the real-time approaches suffer from the rather poor spatial and temporal resolution. For providing high-fidelity images of lung function, Fischer *et al*. (29) have introduced SElf-gated Non-Contrast-Enhanced FUnctional Lung imaging (SENCEFUL), which combines respiratory and cardiac self-gated imaging with subsequent FD for ventilation and perfusion assessment (29). Recently it has been shown that a single free-breathing (FB) data acquisition combining UTE readouts with tyGA encoding schemes (19) is capable of providing the aforementioned function parameters of the lung from a single FB scan (30).

A direct comparison between BH- and FB-derived functional lung parameters and their respective reproducibility has not yet been reported. It is the aim of the presented study to compare BH and FB quantitative functional lung imaging regarding inter-measurement and inter-observer reproducibility in healthy volunteers. We present the following article in accordance with the GRRAS reporting checklist (available at https://qims.amegroups.com/article/view/10.21037/qims-22-92/rc).

Methods

Nine volunteers (mean age 27.7±1.5, 4 females and 5 males) were included in this prospective study. None of the volunteers had a reported history of cardiopulmonary disease or any pulmonary event (such as infection) within one month prior to the examination.

The study was conducted in accordance with the Declaration of Helsinki (as revised in 2013). The study was approved by the institutional ethics board of Ulm University and written informed consent was obtained from all volunteers prior to the examinations.

MR protocol

All measurements were performed using a clinical 3T whole-body MR scanner (Achieva 3T, Philips Healthcare, Best, The Netherlands). Data were acquired in coronal orientation with the integrated 16-channel (4×4) posterior coil in combination with a matching 16-channel (4×4) anterior segment.

Table 1 Parameters for the acquisition of 2D-tyUTE MRI

Parameters	2D-tyUTE MRI	
	BH	FB
Echo time (ms)	0.38	0.38
Repetition time (ms)	6.0	2.0
Flip angle (°)	6	6
Field of view (mm^2)	400×400	400×400
Resolution (mm^2)	2×2	2×2
Slice thickness (mm)	20	20
Number of slices	3	3
Tiny golden angle increment φ_7 (°)	23.62814	23.62814
Acquisition time of T_{ACQ} (sec per slice)	5	84
Oversampling	6	20
Bandwidth (Hz/pixel)	2,184	2,184
Number of readout points	216	216

2D-tyUTE MRI, 2D-tiny golden angle ultrashort echo time magnetic resonance imaging; BH, breath-hold; FB, free-breathing.

The imaging protocol involved 2 examinations (M1, M2) on the same day performed with a short break (<5 min) and repositioning of the volunteer in-between, followed by a third examination (M3) at least 14 days later. The MRI protocol comprised BH and FB acquisitions for a stack of 3 coronal slices acquired from anterior to posterior, with the center slice positioned at the tracheal bifurcation (27).

Radial 2D spoiled center-out tiny golden angle ultrashort echo time (2D-tyUTE) acquisitions were performed according to a previously published protocol (22). In brief, data were acquired in coronal orientation during two BHs in end-EX and end-IN, and continuously during free breathing. Acquisition parameters for the BH and FB acquisitions are given in *Table 1*.

Data reconstruction

Images were reconstructed with an in-house developed reconstruction framework implemented in MatLab (MathWorks, Natick, Massachusetts, USA). To compensate for gradient distortions, the ideal trajectory was convolved with a mono-exponential decay function with a 43 µs time constant. Radial data were resampled onto a Cartesian grid by convolution interpolation and reconstructed by subsequent Fourier-transform. Reconstruction was performed independently for each receive coil and the final image was compiled as the sum-of-squares to avoid any impact of erroneous coil sensitivity pattern in the low signal regions within the lung.

Images in different respiratory phases were reconstructed applying an image-based self-gating technique (11,22,31). The intermediate images were reconstructed with a sliding window technique with a temporal resolution of 400 ms with about 50% temporal overlap between subsequent frames. From this time-series, a navigator-like signal was derived from a manually identified region of interest (ROI) covering the lung-liver interface. For fractional ventilation (FV) calculation, the top and bottom 30% of data were used for reconstruction of expiration (top 30%) and inspiration (bottom 30%) images. For spectral analysis data were sorted into 12 equidistant bins. Due to the limited temporal fidelity of the image-based gating signal, the self-gating signal of cardiac motion was derived from the k-space center (k_0) amplitude (DC) modulation. The coil contributing most considerably to the DC signal modulation was identified according to the amplitude of the cardiac spectral component and used for deriving the respective gating signal, which was filtered with a bandpass filter between 0.75 and 2 Hz (25,29). Data were sorted into 12 equidistant bins covering one cardiac cycle.

Data analysis

The data analysis was performed on magnitude data. The mean noise level $\overline{SI}_{noise}$ was derived from a manually identified artifact-free background 5×5 pixel ROI and subtracted prior to quantitative analysis to avoid a substantial impact of the noise floor to the low-apparent SNR data analysis (32).

Prior to data analysis, the lung parenchyma was segmented semi-automatically thereby carefully excluding larger vessels. Segmentation was performed independently in all images by an active contour method, based on the Chan-Vese technique (33) (Image Segmenter App, MatLab).

For BH and FB, the lung parenchyma voxels apparent *SNR*, lung density (f_P), and FV were quantified (22). In brief, the apparent SNR in the lung parenchyma was calculated as:

$$SNR = \frac{\overline{SI}_{lung}}{\sigma_{noise}} \quad [1]$$

with $\overline{SI}_{lung}$ being the mean value of a 5×5 pixel region and σ_{noise} the standard deviation of the previously identified

background region. f_P was calculated pixelwise as:

$$f_p = \frac{\overline{SI}_{lung}}{\overline{SI}_{muscle}} \cdot \exp\left(\frac{TE}{T_2^*}\right) \quad [2]$$

with $\overline{SI}_{muscle}$ being the intramuscular signal reference derived from a manually identified ROI placed in the intercostal muscle, and T_2^*=0.74 ms used for correcting T_2^* effects caused by the rapid signal decay at 3T (2). The FV (34) was calculated as relative change between IN and EX signal intensities as:

$$FV = \frac{\overline{SI}_{EX} - \overline{SI}_{IN}}{\overline{SI}_{EX}} \quad [3]$$

To ensure a proper match of the lung parenchyma between IN and EX, a nonrigid image registration was performed applying the MIRT—Medical Image Registration Toolbox for MatLab (35) with the sum of squared differences (SSD) as similarity measure in a free form deformation algorithm. All images were registered to the expiration image.

In the FB data, the maximal and minimal lung perfusion was additionally quantified over the cardiac cycle (26,36,37) as:

$$f = \frac{\overline{SI}_{lung}}{\overline{SI}_{blood}} \cdot \frac{1}{2T_{RR}} \quad [4]$$

with $\overline{SI}_{lung}$ being the cardiac phase dependent intensity in the lung, $\overline{SI}_{blood}$ the signal intensity of a completely blood-filled voxel derived from the ROI located in a major vessel (e.g., the aorta), and T_{RR} the length of the cardiac cycle.

Further, ventilation and perfusion maps were derived from FD of the registered respiratory motion and cardiac motion resolved data sets, where ventilation and perfusion contributions were derived from the amplitude of the first frequency component next to DC in the respective spectra as suggested by Fischer *et al.* (29).

The evaluation was performed independently by two blinded observers. Both observers were experienced in the reconstruction and quantitative analysis of lung MRI. Before evaluation, both observers received initial joint training to achieve a consistent evaluation. The inter-measurements differences by the 2 observers as well as inter-observer differences were compared.

Statistical analysis

Images were normalized before analysis and continuous data are shown as mean ± standard deviation. Normality of distribution was tested applying a Kolmogorov-Smirnov test. Statistical significances between the different groups were assessed by using an analysis of variance (ANOVA) test. A P value below 0.05 was considered to be statistically significant. ICCs with measurement of consistency were calculated along with absolute agreement to take the potential systematic variability into account. ICC values indicate poor (<0.50), moderate (≥0.5, <0.75), good (≥0.75, <0.9), or excellent (≥0.9) concordance (38). Bland-Altman plots were used for the evaluation of concordances and to demonstrate reproducibility. Data were analyzed with GraphPad Prism and SPSS (IBM Corporation, Armonk, NY, USA). The similarity between two parameter maps derived either at different time points or with different means was calculated applying the structural similarity index (SSIM).

Results

Feasibility

The MR protocol including BH and FB acquisitions could successfully be performed in all volunteers. Image-based self-gating signals (respiratory motion) and DC self-gating signals (cardiac motion) with sufficient signal fidelity to identify the respiratory and cardiac phases could be obtained from all acquisitions, yielding artifact-free images as shown in *Figure 1*. Example images of the central slice are provided in *Figure 2* for BH and FB acquisitions. Example respiratory and cardiac multi-phase images are provided in the supplementary material (*Videos 1*,*2*). Example registration images are given in the *Video 3*. Lung parenchyma intensity changes over the cardiac- and respiratory cycle can be clearly appreciated (Figure S1).

Quantitative analysis

Larger breathing amplitudes were observed in the BH acquisitions, which also showed lower reproducibility when compared with the FB acquisitions (*Figure 3*). Assessment of apparent SNR, lung density (BH, FB), FV (BH, FB) and perfusion analysis (FB only) was feasible (*Table 2*, *Table 3*) for all measurements. In comparison to inspiration, a significant (P<0.05) increase of lung density and apparent SNR was observed during expiration for BH and FB measurements. Differences between inspiration and expiration resulted more pronounced for BH, which is also reflected in the significant higher FV values observed with BH. End-

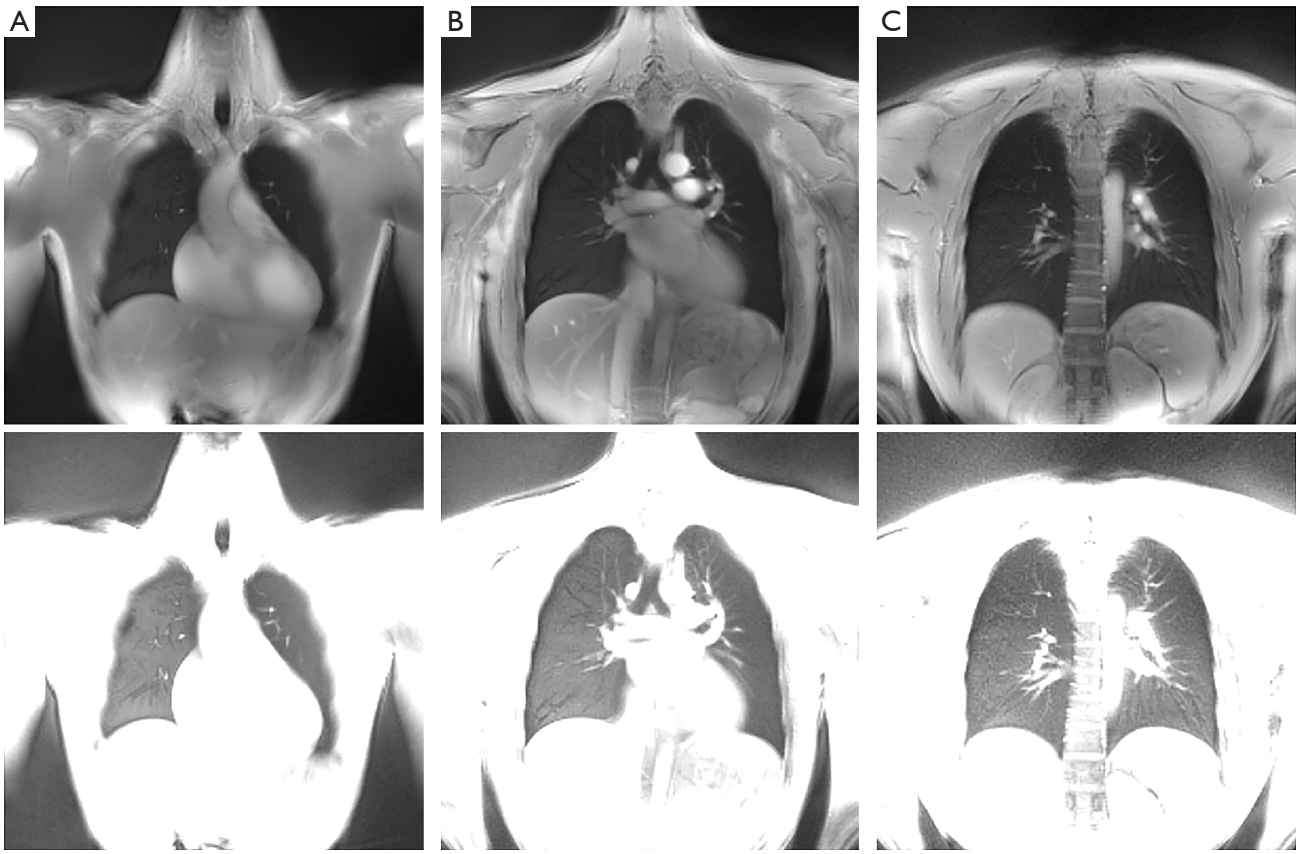

Figure 1 Representative 2D tiny Golden Angle UTE acquired images with different level and window settings to highlight the non-lung (upper row) and lung (bottom row) anatomy. (A) Representative 2D tiny Golden Angle UTE acquired in anterior; (B) representative 2D tiny Golden Angle UTE acquired in middle; (C) representative 2D tiny Golden Angle UTE acquired in posterior. UTE, ultrashort echo-time.

expiration lung densities resulted significantly lower for FB, with no significant (P=0.2) differences during inspiration. Apparent SNR was significantly higher for FB for all analyzed data. In all cases, a clear variation of the perfusion over the cardiac cycle and respective minimum and maximal values ($QPerf_{min/max}$) could be derived.

Inter-measurement reproducibility

In general, the intraclass correlation coefficient (ICC) between M1/2 and M3 resulted lower as between M1 and M2, with superior reproducibility of the FB approach (Table S1, Table S2). With the exception of the FV between M1 and M3 (ICC =0.7), in FB all quantified parameters including lung density, apparent SNR, FV and maximal and minimal perfusion yielded at least good absolute agreement between all three measurements with ICCs ranging between 0.78 and 0.98 (Table S1). Reproducibility for the BH (Table S2) resulted lower with clear limitations especially for the lung density and consequently also for the FV with ICCs ranging between 0.28 and 0.92. apparent SNR revealed ICCs between 0.81 to 0.89. For respective Bland-Altman plots, please refer to Figures S2-S4.

FV maps could be derived from BH and FB acquisitions (*Figure 4*). High SSIMs in the order of 0.9 were observed for FB as well as BH data, whereas lower SSIMs were observed in rare cases of huge differences in the respiratory amplitude, which are not obvious from the displayed mean values in Table S3 and Table S4. FD derived ventilation and perfusion maps could successfully be derived from the respective dynamic image series (*Figure 5*), with rather high SSIMs especially between the 1st and 2nd measurement (Table S5). SSIMs between intensity-based and spectral analysis-based ventilation maps ranged above 0.8, indicating a good concordance of the respiratory maps derived from the two approaches (Table S6).

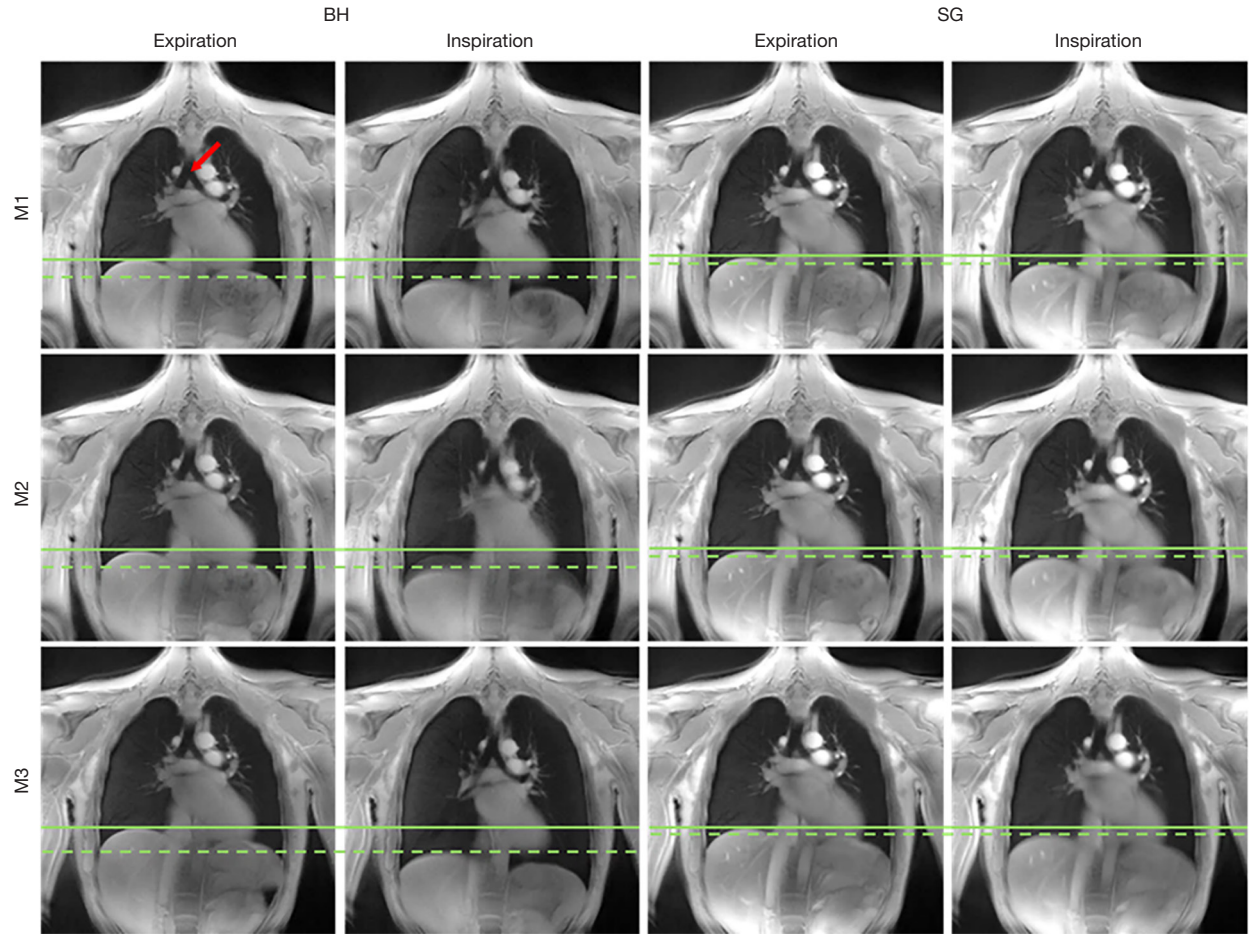

Figure 2 Example of 2D UTE BH (left two columns) and free-breathing with SG (right two columns) lung images for expiration and inspiration for the 3 measurements (M1–3). Red arrow indicates the location of the tracheal bifurcation used for reproducible positioning of the central coronal slice. UTE, ultrashort echo-time; BH, breath-hold; SG, self-gating.

Video 1 Multi-cardiac phase images reconstructed from a continuous tyGA acquisition during free breathing. Images were reconstructed applying k0-based self-gating technique. tyGA, tiny golden angle.

Video 2 Respiratory phase images reconstructed from a continuous tyGA acquisition during free breathing. Images were reconstructed applying an image-based self-gating technique. tyGA, tiny golden angle.

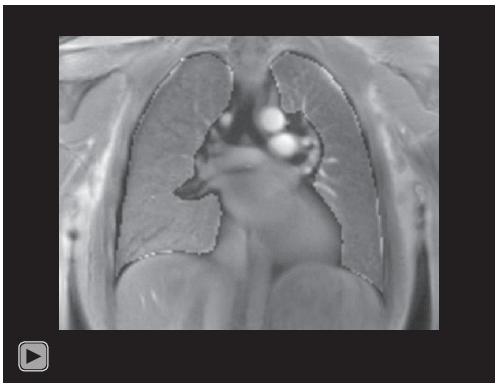

Video 3 Images show the segmented lung over the respiratory cycle after segmentation and registration to the end-expiratory reference phase. Image contrast has been adjusted for lung parenchyma visualization.

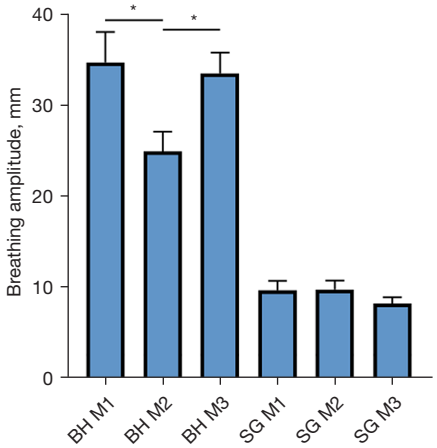

Figure 3 Breathing amplitude for the BH and FB acquisitions for the three measurements (M1–3). *, statistical significance. BH, breath-hold; FB, free-breathing; SG, self-gating.

Table 2 Quantitative lung parameters derived from the breath-hold measurements M1–3 and observers 1 and 2

Observers	Respiratory phase	Measurement 1	Measurement 2	Measurement 3
Observer 1				
Lung density	EX	0.43±0.07	0.43±0.08	0.41±0.05
	IN	0.37±0.08	0.40±0.07	0.36±0.06
Signal-to-Noise	EX	21.17±9.57	20.75±8.75	19.48±7.48
	IN	18.14±8.85	17.51±7.50	15.99±6.49
Fractional Ventilation		0.15±0.06	0.12±0.04	0.16±0.06
Observer 2				
Lund density	EX	0.42±0.06	0.42±0.06	0.40±0.05
	IN	0.37±0.07	0.39±0.06	0.35±0.06
Signal-to-Noise	EX	21.40±9.56	20.98±8.66	19.96±7.68
	IN	18.37±8.62	17.69±7.44	15.64±6.24
Fractional Ventilation		0.16±0.06	0.12±0.04	0.16±0.06

EX, expiration; IN, inspiration.

Inter-observer reproducibility

For BH, excellent inter-observer agreement was obtained for FV (ICC =0.97) and apparent SNR (ICC =0.99), but only good agreement for the lung density (ICC =0.76–0.79) (*Table 4*). In FB excellent inter-observer agreements resulted for lung density, apparent SNR and FV with ICCs ranging from 0.90 to 0.97, and good agreement (ICC =0.86) for the quantitative perfusion assessment (*Table 5*). For respective Bland-Altman plots, please refer to Figures S5,S6.

Discussion

Methods providing quantitative regional information are needed because many lung diseases present with a highly heterogeneous pattern. Compared to computed tomography (CT), especially considering the limitation in pediatric applications, MRI provides not only morphologic but also functional information with nonionizing radiation. This may be especially important for early detection of disease and for continuous therapy monitoring.

Table 3 Quantitative lung parameters derived from the free-breathing measurements 1–3 and observers 1 and 2

Observers	Respiratory phase	Measurement 1	Measurement 2	Measurement 3
Observer 1				
Lung density	EX	0.37±0.08	0.38±0.07	0.36±0.05
	IN	0.35±0.08	0.36±0.07	0.34±0.05
Signal-to-Noise	EX	29.51±12.94	26.51±9.07	27.97±9.04
	IN	24.93±9.41	25.20±9.15	25.97±9.34
Fractional Ventilation		0.08±0.03	0.08±0.03	0.07±0.03
$QPerf_{max}$		4.74±1.02	4.70±1.08	4.76±1.09
$QPerf_{min}$		4.41±1.09	4.41±1.12	4.38±1.12
Observer 2				
Lung density	EX	0.37±0.09	0.37±0.08	0.36±0.06
	IN	0.36±0.08	0.35±0.08	0.34±0.06
Signal-to-Noise	EX	28.70±11.51	28.02±9.91	27.54±7.27
	IN	25.52±9.78	25.48±7.65	24.65±7.86
Fractional Ventilation		0.07±0.03	0.08±0.03	0.07±0.02
$QPerf_{max}$		5.01±1.20	4.89±1.18	5.08±0.96
$QPerf_{min}$		4.66±1.15	4.56±1.17	4.78±1.01

EX, expiration; IN, inspiration; $QPerf_{max}$, maximum perfusion value over the cardiac cycle; $QPerf_{min}$, minimum perfusion value over the cardiac cycle.

Discussion of quantitative results

In this study, the reproducibility of MRI-derived lung parameters based on BH and FB 2D-tyUTE was investigated. In general, good to excellent reproducibility of the quantitative lung density (BH, FB), FV (BH, FB), and peak perfusion (FB) could be shown as well as for the more qualitative spectral analysis of ventilation and perfusion induced signal changes in the lung parenchyma (FB) as assessed by the SSIM.

No bias over time was found for all quantitative parameters in healthy volunteers between three measurements repeated within 2 h and 14 d. The expected differences in the lung parenchyma signal intensity between expiration and inspiration (BH, FB) and over the cardiac and respiratory cycle (FB) were clearly visible. The ICC of inter-measurement and inter-observer test as well as Bland- Altman analysis showed good agreement demonstrating the reproducibility of the assessed quantitative and qualitative lung parameters.

As shown in a previously reported study (39), tidal volume variability is a critical factor for FV reproducibility. This was clearly confirmed by our data indicating a limited reproducibility of the tidal volume and hence of the derived parameters which rely on reproducible breathing amplitude such as FV and lung density. This was clearly reduced with the FB technique in which only small differences in tidal amplitudes between the three measurements were observed; however with on average clearly reduced respiratory amplitudes and resulting lower differences in the lung parenchyma intensities between inspiration and expiration. For FB, the 2D tyGA UTE sequence appeared of special advantage due to its unique k-space filling which ensured high flexibility regarding trading spatial *vs.* temporal resolution with simultaneous continuous update of the k-space center intensity. This enables high flexibility for image-based and/or center of k-space based gating as well as real-time reconstructions from the same data set, which may be applied for deriving high-quality multi-phase cardiac and respiratory images from the gated data as well as real-time data, both of which might be applied to spectral analysis of cardiac and respiratory induced signal intensity changes of the lung parenchyma (29).

Differences in the pattern of the FV and FD ventilation maps can be explained by the different underlying

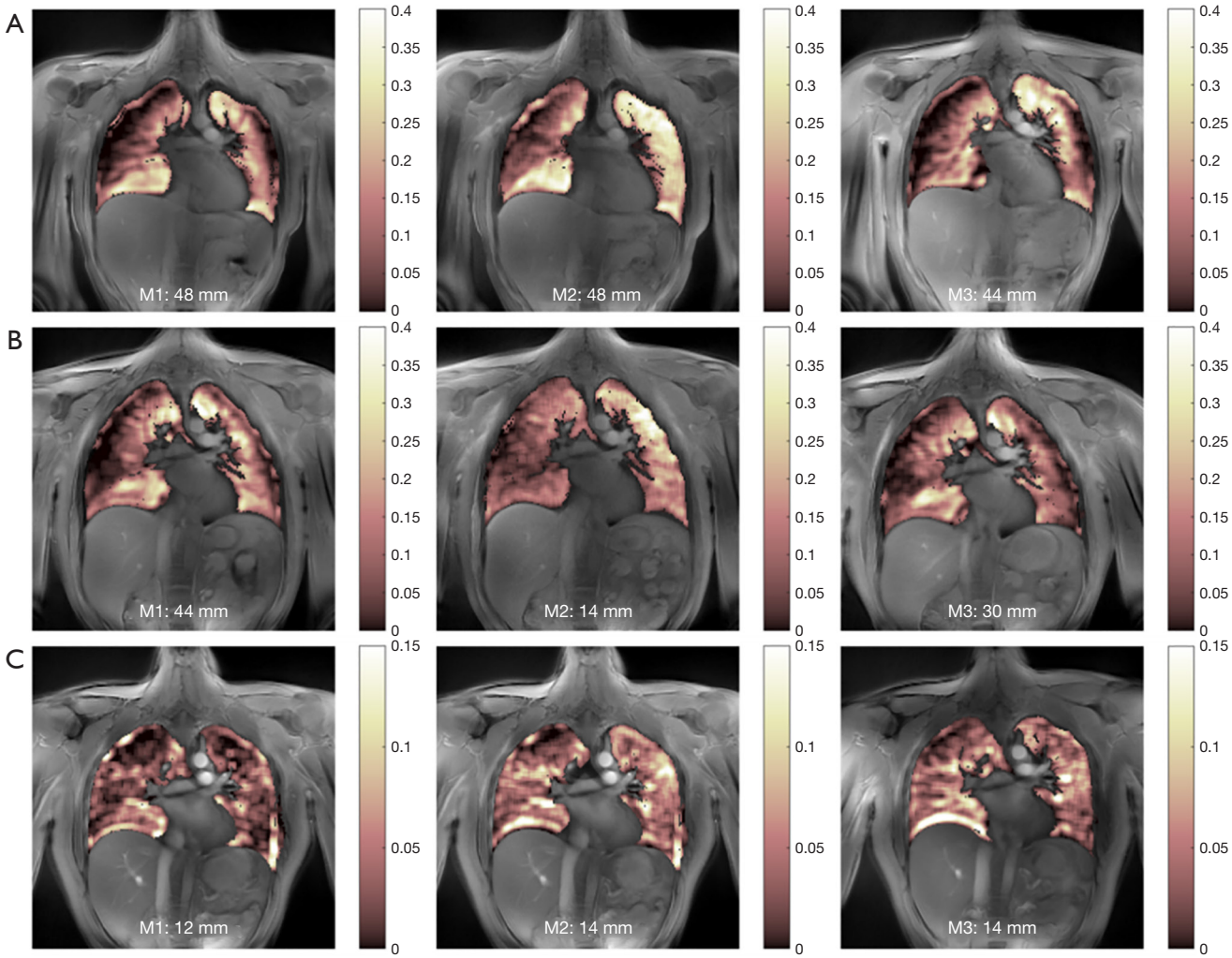

Figure 4 FV maps of BH and FB for a volunteer. (A) FV maps of BH with reproducible breathing amplitude; (B) FV maps of BH with non-reproducible breathing amplitude; (C) FV maps of FB. FV, fractional ventilation; BH, breath-hold; FB, free-breathing.

methodology. While FV is calculated from only two images including a noise-sensitive division operation, FD techniques use images over the entire respiratory cycle, which as such may ensure less impact of the noise on the resulting image; however with the penalty of an increased computational effort as more frames need to be registered. While the FD-derived maps appear more convincing, both methods seem to map the same structures, as can be seen from the SSIM values.

Limitations

Even though the presented study implies a high reproducibility of the investigated 2D tyGA approach, clear limitations are rising from the currently still limited spatial resolution especially in slice selection direction. A possible alternative is the use of modified 3D-UTE Kooshball trajectories as presented elsewhere (10,11). 3D imaging could also mitigate problems of reproducibility concerning the patient positioning. As this study was conducted with 2D acquisitions, retrospective reformatting of data was not possible and differences in patient positioning could have led to slightly different imaging regions (e.g., elevated upper body, tilting of the imaging plane).

The implicit assumption of a linear relationship of the lung parenchyma signal intensity changes with ventilation-induced local volume changes does not reflect any related changes of T_2* likely occurring due to changes in the air-

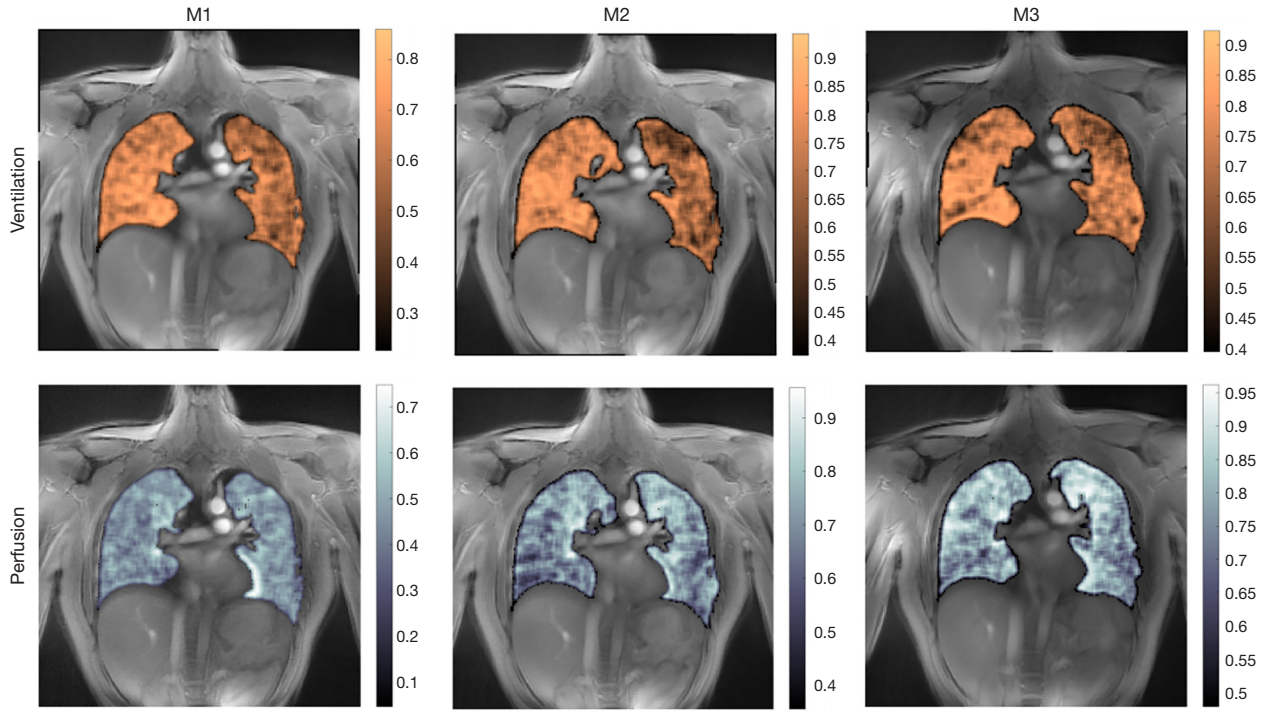

Figure 5 Ventilation and perfusion map derived from spectral analysis of the dynamic cardiac (perfusion) and respiratory (ventilation) time series. M1–3, Measurements 1–3.

Table 4 ICC between the two observers for the breath-hold measurements

Parameters	Respiratory phase	Inter-observer ICC (95% CI)
Lung density	EX	0.76 (0.63–0.85)
	IN	0.79 (0.67–0.86)
Signal-to-noise	EX	0.99 (0.98–0.99)
	IN	0.99 (0.99–0.99)
Fractional ventilation		0.97 (0.95–0.98)

ICC, intraclass correlation coefficient; EX, expiration; IN, inspiration.

Table 5 ICC between the two observers for the free-breathing measurements

Parameters	Respiratory phase	Inter-observer ICC (95% CI)
Lung density	EX	0.97(0.96–0.98)
	IN	0.97(0.95–0.98)
Signal-to-noise	EX	0.93(0.88–0.95)
	IN	0.91(0.86–0.94)
Fractional ventilation		0.90(0.84–0.94)
QPerf		0.86(0.79–0.91)

ICC, intraclass correlation coefficient; EX, expiration; IN, inspiration; QPerf, perfusion value.

tissue interfaces, and must be interpreted as a first order approximation. Similar care must be taken for proper interpretation of the lung density values. The calculated value is dependent on proper identification of a muscle reference signal and correct consideration of the lung parenchymal T_2* value. Both values may be impacted e.g., by coil-sensitivity pattern and B0 and B1 inhomogeneities. Inclusion of coil-sensitivity patterns in the analysis is—in our experience—not as straight-forward as it might seem. The respiratory motion, especially during large respiratory amplitudes as present during BHs, will likely displace the anterior coil elements. To not introduce inaccuracies, respiration-dependent coilmaps would have to be used. However, with rather low reproducibility of BH positions (especially in patients) and the additional burden of a higher number of BHs, standard approaches might not be feasible. An alternative could be image-based sensitivity calculations (40), which have already been used in the lung context (41).

Further, for functional assessment segmentation of the lung parenchyma and registration between the different respiratory phases is required to avoid falsified results by partial volume effects or blood vessels and comparison of nonmatching lung parenchyma (25,29). Segmentation and registration are intrinsically prone to be inaccurate and careful check is required to ensure proper and reproducible results. The use of the semiautomatic approaches as proposed in this study are time-consuming and may not be suited for larger clinical studies or clinical routines. However, with the upcoming deep-learning techniques this limitation may be addressed.

Considering that data analysis is normally performed on magnitude data, the noise floor may mimic higher signal in the lung parenchyma and hence also impact derived parameters, and background noise correction is recommended (22). Here the identification of an artifact-free background region is of utmost importance to avoid any impact of rising aliasing artifacts on the data analysis. In this study, the subtracted noise floor was approximated as the mean of the artifact-free background region. However, as Gudbjartsson and Pratz (42) have demonstrated, noise in this low signal region is Rician and the noise power could be derived with a correction factor, thus leading to a correction formula ensuring a mathematically stricter treatment of the noise correction. However, although this will change the numerical values, the main statement of this publication regarding repeatability and regional differences will not be affected.

Although manual selection of appropriate coil elements for the derivation of the self-gating signal is widely used in literature (43,44), it might be beneficial to use a global channel reduction (31) or an automatic procedure to select the optimal channel (45). Automation of frequency analysis seems to be more difficult because the non-sinusoidal nature of respiration may lead to harmonics that could possibly be mistaken for cardiac motion.

In this study, even though reproducible, on average lung densities resulted higher as expected. This as such should not dramatically impact the derived function parameters or the assessment of lung density changes as caused e.g., by infiltrates or infections, but needs consideration if absolute lung densities are compared between subsequent measurements or between different patients.

Further limitations of this study include the rather low number of volunteers and the lack of patients with pathologic changes to also assess the sensitivity of the proposed technique. However, other groups have already reported quite good sensitivity of the general idea of MR-derived lung function parameters. Despite all the mentioned limitations, considering the high reproducibility shown for the 2D tyGA UTE technique in this study, it may contribute to further translation of lung MRI into the clinics.

As mentioned above, major limitations still rise to form the limited automatization of the required data analysis. Even though partly available e.g., with the PREFUL technique, further improvements, especially in the robustness of the technique, are expected from further progress in the field of deep-learning especially for supporting the required segmentation and registration.

Conclusions

The FB 2D tyGA UTE appears to be a promising technique for lung imaging. Ventilation and perfusion maps derived from SENCEFUL and functional parameters are repeatable in healthy volunteers which may be useful in the clinical setting to non-invasively monitor patients with lung disease in the future.

Acknowledgments

Funding: This work was partly funded by a research grant of German Research Foundation (No. 465599659, to VR), and Boehringer Ingelheim (to VR and MB). The funding parties were not involved in the study design, manuscript writing, editing, approval, or decision to publish.

Footnote

Reporting Checklist: The authors have completed the GRRAS reporting checklist. Available at https://qims.amegroups.com/article/view/10.21037/qims-22-92/rc

Conflicts of Interest: All authors have completed the ICMJE uniform disclosure form (available at https://qims.amegroups.com/article/view/10.21037/qims-22-92/coif). BY reports that she was supported by the China Scholarship Council (CSC). VR and MB report that this work was partly funded by a research grant of German Research Foundation (No. 465599659, to VR), and Boehringer Ingelheim (to VR and MB). The funding parties were not involved in the study design, manuscript writing, editing, approval, or decision to publish. The other authors have no conflicts of interest to declare.

Ethical Statement: The authors are accountable for all aspects of the work in ensuring that questions related to the accuracy or integrity of any part of the work are appropriately investigated and resolved. The study was conducted in accordance with the Declaration of Helsinki (as revised in 2013). The study was approved by the institutional ethics board of Ulm University and written informed consent was obtained from all volunteers prior to the examinations.

References

1. Wild JM, Marshall H, Bock M, Schad LR, Jakob PM, Puderbach M, Molinari F, Van Beek EJ, Biederer J. MRI of the lung (1/3): methods. Insights Imaging 2012;3:345-53.
2. Yu J, Xue Y, Song HK. Comparison of lung T2* during free-breathing at 1.5 T and 3.0 T with ultrashort echo time imaging. Magn Reson Med 2011;66:248-54.
3. Theilmann RJ, Arai TJ, Samiee A, Dubowitz DJ, Hopkins SR, Buxton RB, Prisk GK. Quantitative MRI measurement of lung density must account for the change in T(2) (*) with lung inflation. J Magn Reson Imaging 2009;30:527-34.
4. Biederer J, Beer M, Hirsch W, Wild J, Fabel M, Puderbach M, Van Beek EJ. MRI of the lung (2/3). Why … when … how? Insights Imaging 2012;3:355-71.
5. Puderbach M, Hintze C, Ley S, Eichinger M, Kauczor HU, Biederer J. MR imaging of the chest: a practical approach at 1.5T. Eur J Radiol 2007;64:345-55.
6. Hatabu H, Alsop DC, Listerud J, Bonnet M, Gefter WB. T2* and proton density measurement of normal human lung parenchyma using submillisecond echo time gradient echo magnetic resonance imaging. Eur J Radiol 1999;29:245-52.
7. Bae K, Jeon KN, Hwang MJ, Lee JS, Ha JY, Ryu KH, Kim HC. Comparison of lung imaging using three-dimensional ultrashort echo time and zero echo time sequences: preliminary study. Eur Radiol 2019;29:2253-62.
8. Johnson KM, Fain SB, Schiebler ML, Nagle S. Optimized 3D ultrashort echo time pulmonary MRI. Magn Reson Med 2013;70:1241-50.
9. Zhu X, Chan M, Lustig M, Johnson KM, Larson PEZ. Iterative motion-compensation reconstruction ultra-short TE (iMoCo UTE) for high-resolution free-breathing pulmonary MRI. Magn Reson Med 2020;83:1208-21.
10. Mendes Pereira L, Wech T, Weng AM, Kestler C, Veldhoen S, Bley TA, Köstler H. UTE-SENCEFUL: first results for 3D high-resolution lung ventilation imaging. Magn Reson Med 2019;81:2464-73.
11. Tibiletti M, Paul J, Bianchi A, Wundrak S, Rottbauer W, Stiller D, Rasche V. Multistage three-dimensional UTE lung imaging by image-based self-gating. Magn Reson Med 2016;75:1324-32.
12. Tibiletti M, Kjørstad Å, Bianchi A, Schad LR, Stiller D, Rasche V. Multistage self-gated lung imaging in small rodents. Magn Reson Med 2016;75:2448-54.
13. Ma W, Sheikh K, Svenningsen S, Pike D, Guo F, Etemad-Rezai R, Leipsic J, Coxson HO, McCormack DG, Parraga G. Ultra-short echo-time pulmonary MRI: evaluation and reproducibility in COPD subjects with and without bronchiectasis. J Magn Reson Imaging 2015;41:1465-74.
14. Lederlin M, Crémillieux Y. Three-dimensional assessment of lung tissue density using a clinical ultrashort echo time at 3 tesla: a feasibility study in healthy subjects. J Magn Reson Imaging 2014;40:839-47.
15. Weiger M, Wu M, Wurnig MC, Kenkel D, Jungraithmayr W, Boss A, Pruessmann KP. Rapid and robust pulmonary proton ZTE imaging in the mouse. NMR Biomed

2014;27:1129-34.
16. Takizawa M, Hanada H, Oka K, Takahashi T, Yamamoto E, Fujii M. A robust ultrashort TE (UTE) imaging method with corrected k-space trajectory by using parametric multiple function model of gradient waveform. IEEE Trans Med Imaging 2013;32:306-16.
17. Glover GH, Pauly JM. Projection reconstruction techniques for reduction of motion effects in MRI. Magn Reson Med 1992;28:275-89.
18. Wundrak S, Paul J, Ulrici J, Hell E, Rasche V. A Small Surrogate for the Golden Angle in Time-Resolved Radial MRI Based on Generalized Fibonacci Sequences. IEEE Trans Med Imaging 2015;34:1262-9.
19. Wundrak S, Paul J, Ulrici J, Hell E, Geibel MA, Bernhardt P, Rottbauer W, Rasche V. Golden ratio sparse MRI using tiny golden angles. Magn Reson Med 2016;75:2372-8.
20. Radbruch A. Gadolinium Deposition in the Brain: We Need to Differentiate between Chelated and Dechelated Gadolinium. Radiology 2018;288:434-5.
21. Kern AL, Vogel-Claussen J. Hyperpolarized gas MRI in pulmonology. Br J Radiol 2018;91:20170647.
22. Balasch A, Metze P, Stumpf K, Beer M, Büttner SM, Rottbauer W, Speidel T, Rasche V. 2D Ultrashort Echo-Time Functional Lung Imaging. J Magn Reson Imaging 2020;52:1637-44.
23. Heidenreich JF, Weng AM, Metz C, Benkert T, Pfeuffer J, Hebestreit H, Bley TA, Köstler H, Veldhoen S. Three-dimensional Ultrashort Echo Time MRI for Functional Lung Imaging in Cystic Fibrosis. Radiology 2020;296:191-9.
24. Glandorf J, Klimeš F, Voskrebenzev A, Gutberlet M, Behrendt L, Crisosto C, Wacker F, Ciet P, Wild JM, Vogel-Claussen J. Comparison of phase-resolved functional lung (PREFUL) MRI derived perfusion and ventilation parameters at 1.5T and 3T in healthy volunteers. PLoS One 2020;15:e0244638.
25. Bauman G, Puderbach M, Deimling M, Jellus V, Chefd'hotel C, Dinkel J, Hintze C, Kauczor HU, Schad LR. Non-contrast-enhanced perfusion and ventilation assessment of the human lung by means of fourier decomposition in proton MRI. Magn Reson Med 2009;62:656-64.
26. Kjørstad Å, Corteville DM, Fischer A, Henzler T, Schmid-Bindert G, Zöllner FG, Schad LR. Quantitative lung perfusion evaluation using Fourier decomposition perfusion MRI. Magn Reson Med 2014;72:558-62.
27. Pöhler GH, Klimeš F, Behrendt L, Voskrebenzev A, Gonzalez CC, Wacker F, Hohlfeld JM, Vogel-Claussen J. Repeatability of Phase-Resolved Functional Lung (PREFUL)-MRI Ventilation and Perfusion Parameters in Healthy Subjects and COPD Patients. J Magn Reson Imaging 2021;53:915-27.
28. Klimeš F, Voskrebenzev A, Gutberlet M, Kern AL, Behrendt L, Grimm R, Suhling H, Crisosto CG, Kaireit TF, Pöhler GH, Glandorf J, Wacker F, Vogel-Claussen J. 3D phase-resolved functional lung ventilation MR imaging in healthy volunteers and patients with chronic pulmonary disease. Magn Reson Med 2021;85:912-25.
29. Fischer A, Weick S, Ritter CO, Beer M, Wirth C, Hebestreit H, Jakob PM, Hahn D, Bley T, Köstler H. SElf-gated Non-Contrast-Enhanced FUnctional Lung imaging (SENCEFUL) using a quasi-random fast low-angle shot (FLASH) sequence and proton MRI. NMR Biomed 2014;27:907-17.
30. Balasch A, Metze P, Li H, Rottbauer W, Abaei A, Rasche V. Tiny golden angle ultrashort echo-time lung imaging in mice. NMR Biomed 2021;34:e4591.
31. Paul J, Divkovic E, Wundrak S, Bernhardt P, Rottbauer W, Neumann H, Rasche V. High-resolution respiratory self-gated golden angle cardiac MRI: Comparison of self-gating methods in combination with k-t SPARSE SENSE. Magn Reson Med 2015;73:292-8.
32. Balasch A, Büttner MS, Metze P, Stumpf K, Beer M, Rottbauer W, Rasche V. Tiny golden angle stack-of-stars (tygaSoS) free-breathing functional lung imaging. Magn Reson Imaging 2021;82:24-30.
33. Chan TF, Vese LA. Active contours without edges. IEEE Trans Image Process 2001;10:266-77.
34. Zapke M, Topf HG, Zenker M, Kuth R, Deimling M, Kreisler P, Rauh M, Chefd'hotel C, Geiger B, Rupprecht T. Magnetic resonance lung function--a breakthrough for lung imaging and functional assessment? A phantom study and clinical trial. Respir Res 2006;7:106.
35. Myronenko A. MIRT - Medical Image Registration Toolbox for Matlab 2018. Available online: https://sites.google.com/site/myronenko/research/mirt
36. Fischer A, Pracht ED, Arnold JF, Kotas M, Flentje M, Jakob PM. Assessment of pulmonary perfusion in a single shot using SEEPAGE. J Magn Reson Imaging 2008;27:63-70.
37. Pracht ED, Fischer A, Arnold JF, Kotas M, Flentje M, Jakob PM. Single-shot quantitative perfusion imaging of the human lung. Magn Reson Med 2006;56:1347-51.
38. Koo TK, Li MY. A Guideline of Selecting and Reporting Intraclass Correlation Coefficients for Reliability Research. J Chiropr Med 2016;15:155-63.

39. Klimeš F, Voskrebenzev A, Gutberlet M, Kern A, Behrendt L, Kaireit TF, Czerner C, Renne J, Wacker F, Vogel-Claussen J. Free-breathing quantification of regional ventilation derived by phase-resolved functional lung (PREFUL) MRI. NMR Biomed 2019;32:e4088.
40. Bydder M, Larkman DJ, Hajnal JV. Combination of signals from array coils using image-based estimation of coil sensitivity profiles. Magn Reson Med 2002;47:539-48.
41. Meadus WQ, Stobbe RW, Grenier JG, Beaulieu C, Thompson RB. Quantification of lung water density with UTE Yarnball MRI. Magn Reson Med 2021;86:1330-44.
42. Gudbjartsson H, Patz S. The Rician distribution of noisy MRI data. Magn Reson Med 1995;34:910-4.
43. Weick S, Breuer FA, Ehses P, Völker M, Hintze C, Biederer J, Jakob PM. DC-gated high resolution three-dimensional lung imaging during free-breathing. J Magn Reson Imaging 2013;37:727-32.
44. Buerger C, Prieto C, Schaeffter T. Highly efficient 3D motion-compensated abdomen MRI from undersampled golden-RPE acquisitions. MAGMA 2013;26:419-29.
45. Grimm R, Bauer S, Kiefer B, Hornegger J, Block T. editors. Optimal channel selection for respiratory self-gating signals. Proc 21st Annual Meeting ISMRM, Salt Lake City, Utah, USA; 2013.

Cite this article as: Yang B, Metze P, Balasch A, Stumpf K, Beer M, Rottbauer W, Rasche V. Reproducibility of functional lung parameters derived from free-breathing non-contrast-enhanced 2D ultrashort echo-time. Quant Imaging Med Surg 2022;12(10):4720-4733. doi: 10.21037/qims-22-92

Supplementary

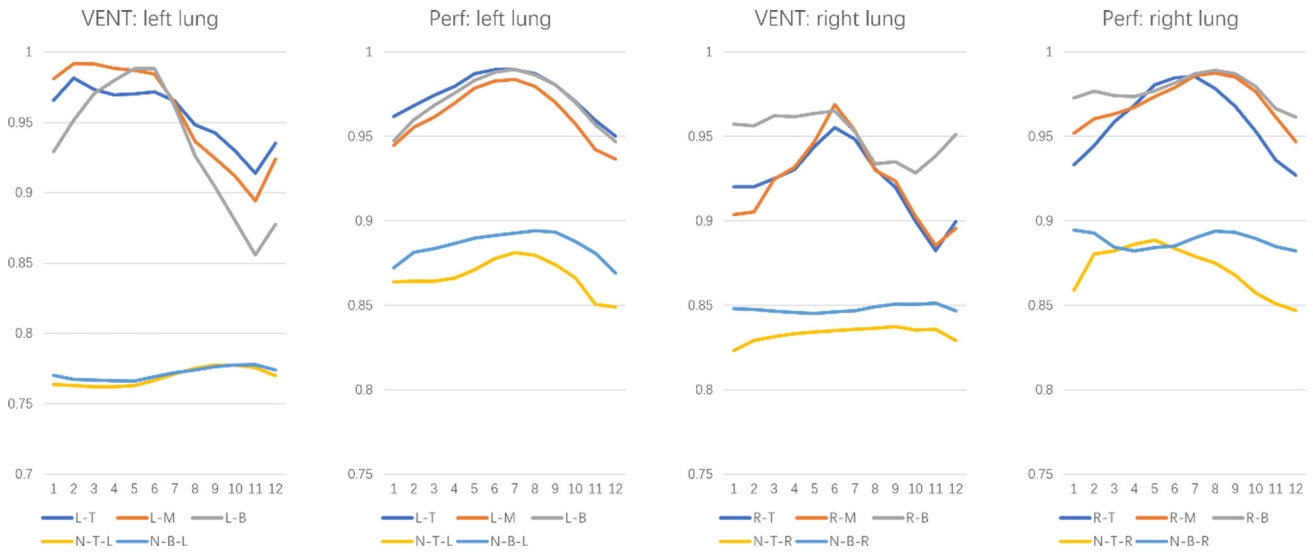

Figure S1 Signal intensity changes over the respiratory (VENT) and cardiac (Perf) cycle at different positions within the parenchyma (left-top (L-T), left-middle (L-M), left-bottom (L-B), right-top (R-T), right-middle (R-M), and right-bottom (R-B) and noise regions (left-top (N-T-L), left-bottom (N-B-L), right-top (N-T-R), right-bottom (N-B-R). Frame 6 corresponds to end-expiration in the ventilation analysis, frame 7 corresponds to the end-systolic phase of the cardiac cycle in the perfusion analysis. For easier comparison, the data were normalized by the maximal ventilation and perfusion value. Noise data was additionally shifted by about 0.5 for better appreciation of shape differences within the lung parenchyma and noise regions.

https://dx.doi.org/10.21037/qims-22-92

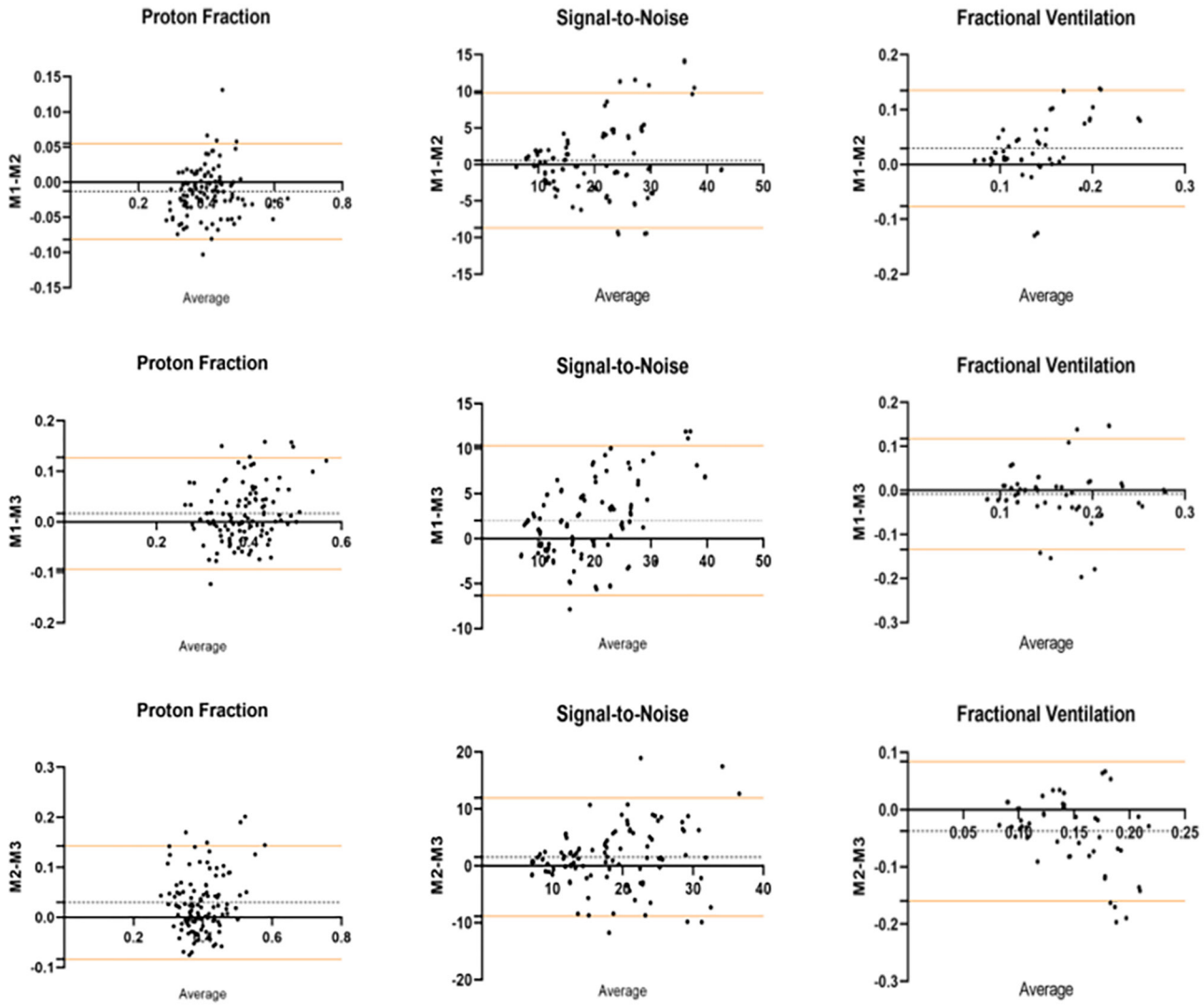

Figure S2 Bland-Altman analysis of the differences between the repeated measurements of lung density, signal-to-noise, and fractional ventilation derived from breath-hold data.

https://dx.doi.org/10.21037/qims-22-92

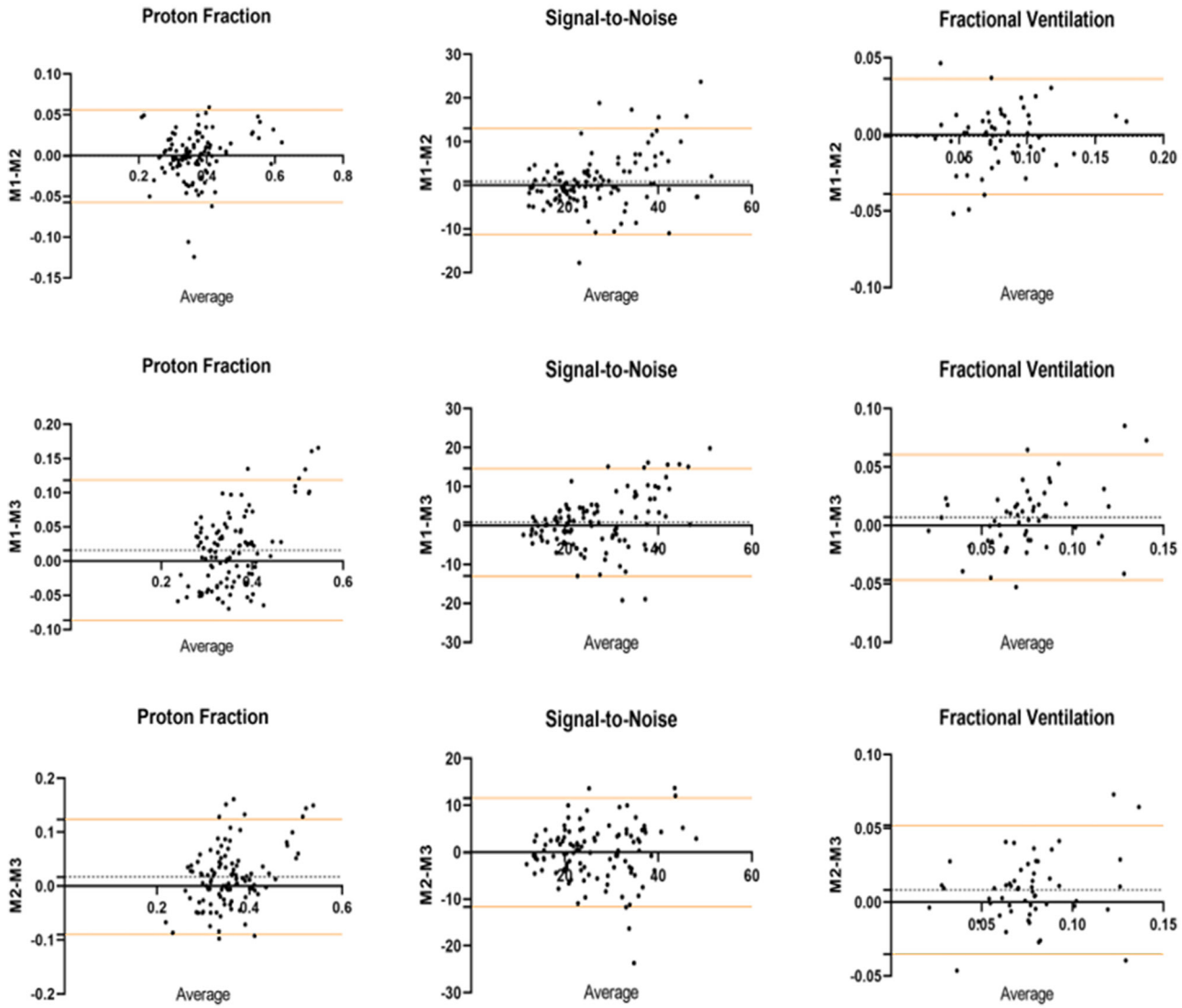

Figure S3 Bland-Altman analysis of the differences between the repeated measurements of lung density, signal-to-noise, and fractional ventilation derived from free-breathing data.

https://dx.doi.org/10.21037/qims-22-92

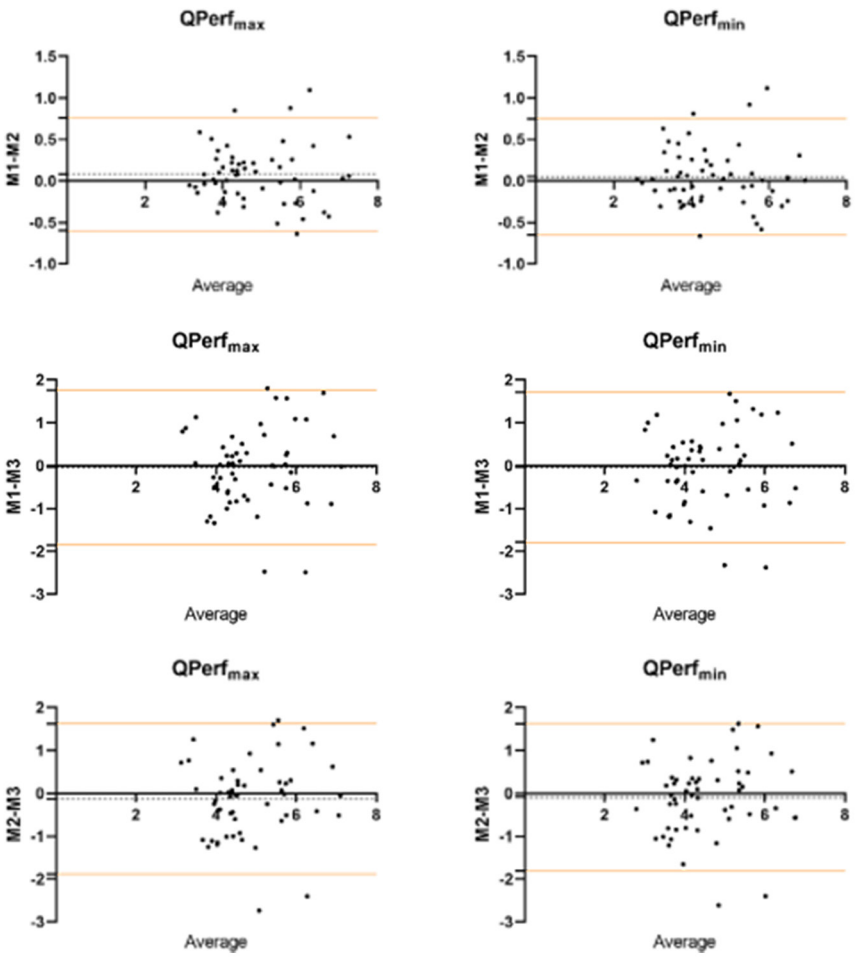

Figure S4 Bland-Altman analysis of the differences between the repeated measurements of lung density, signal-to-noise, fractional ventilation derived from free-breathing data. QPerfmax: maximum perfusion value over the cardiac cycle; QPerfmin: minimum perfusion value over the cardiac cycle.

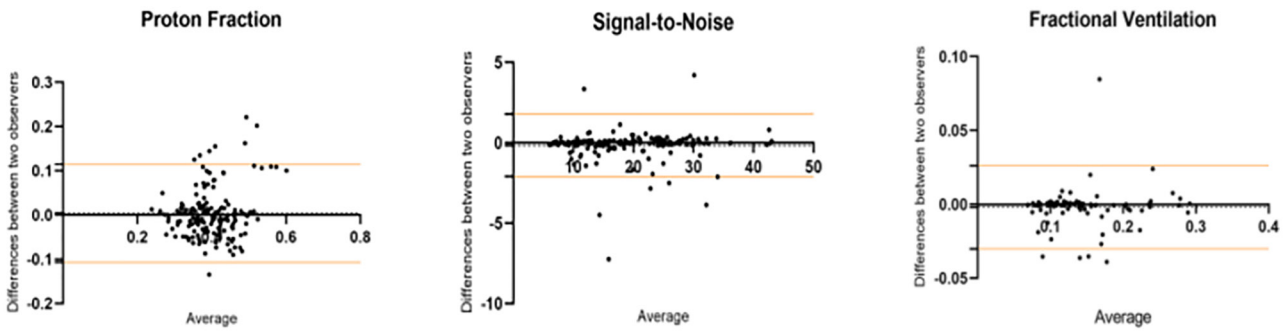

Figure S5 Bland-Altman analysis of the differences between the two observers for lung density, signal-to-noise, and fractional ventilation derived from breath-hold data.

https://dx.doi.org/10.21037/qims-22-92

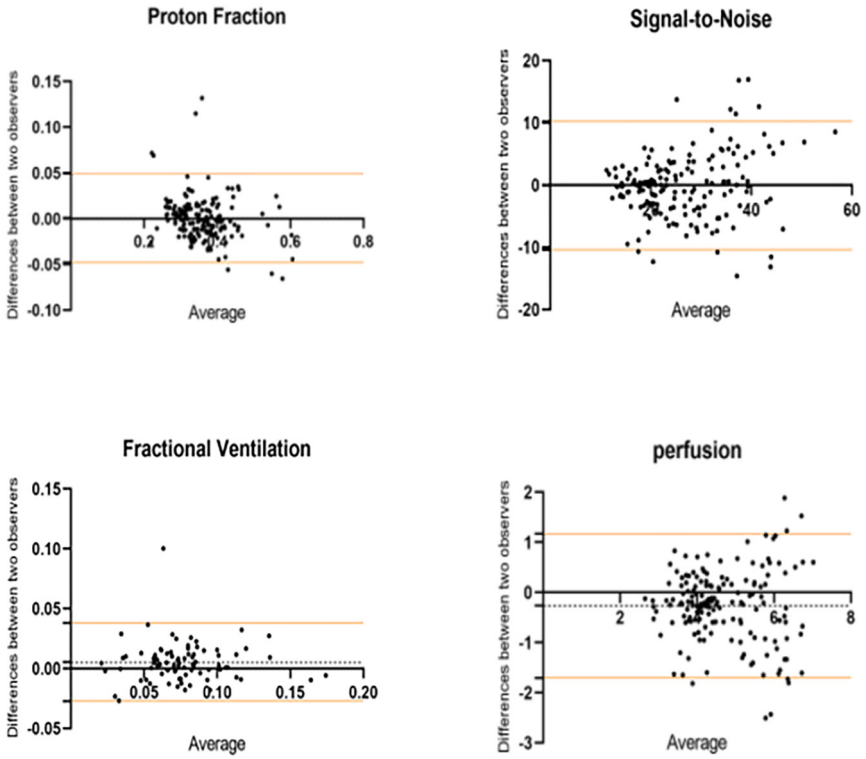

Figure S6 Bland-Altman analysis of the differences between the two observers for lung density, signal-to-noise, fractional ventilation and perfusion derived from free-breathing data.

Table S1 Intraclass correlation coefficient between the three free-breathing measurements

Parameters	Respiratory phase	M1 *vs*. M2	M1 *vs*. M3	M2 *vs*. M3
Lung density	EX	0.97 (0.95; 0.98)	0.82 (0.68; 0.89)	0.77 (0.60; 0.87)
	IN	0.96 (0.93; 0.98)	0.83 (0.70; 0.90)	0.80 (0.64; 0.88)
Signal-to-Noise	EX	0.87 (0.78; 0.93)	0.85 (0.75; 0.92)	0.89 (0.81; 0.94)
	IN	0.92 (0.87; 0.95)	0.85 (0.74; 0.91)	0.85 (0.74; 0.91)
Fractional ventilation		0.90 (0.82; 0.94)	0.70 (0.48; 0.87)	0.78 (0.60; 0.88)
$QPerf_{max}$		0.98 (0.96; 0.99)	0.78 (0.61; 0.87)	0.79 (0.64; 0.88)
$QPerf_{min}$		0.97 (0.86; 0.99)	0.80 (0.66; 0.89)	0.82 (0.68; 0.89)

https://dx.doi.org/10.21037/qims-22-92

Table S2 Intraclass correlation coefficient between the three breath-hold measurements

Parameters	Respiratory phase	M1 *vs.* M2	M1 *vs.* M3	M2 *vs.* M3
Lung density	EX	0.92 (0.87; 0.95)	0.69 (0.46; 0.82)	0.70 (0.47; 0.83)
	IN	0.81 (0.59; 0.90)	0.60 (0.40; 0.75)	0.66 (0.27; 0.83)
Signal-to-Noise	EX	0.82 (0.71; 0.89)	0.86 (0.75; 0.92)	0.83 (0.72; 0.90)
	IN	0.89 (0.81; 0.93)	0.81 (0.59; 0.91)	0.88 (0.71; 0.94)
Fractional ventilation		0.52 (0.16; 0.73)	0.58 (0.27; 0.75)	0.28 (0.14; 0.56)

Table S3 Structural similarity index of Fractional ventilation from BH of 3 measurements

Parameter	Slice	M1 *vs.* M2	M1 *vs.* M3	M2 *vs.* M3
Fractional ventilation	Anterior	0.94±0.02	0.85±0.03	0.85±0.03
	Middle	0.92±0.03	0.81±0.05	0.80±0.05
	Posterior	0.92±0.03	0.80±0.05	0.80±0.05

Table S4 Structural similarity index of fractional ventilation from FB of 3 measurements

Parameter	Slice	M1 *vs.* M2	M1 *vs.* M3	M2 *vs.* M3
Fractional ventilation	Anterior	0.92±0.04	0.84±0.02	0.84±0.02
	Middle	0.92±0.02	0.78±0.05	0.79±0.05
	Posterior	0.91±0.02	0.79±0.04	0.79±0.04

Table S5 Structural similarity index of ventilation and perfusion map (derived from spectral analysis)

Maps	Slice	M1 *vs.* M2	M1 *vs.* M3	M2 *vs.* M3
Ventilation map	Anterior	0.94±0.01	0.86±0.05	0.86±0.05
	Middle	0.91±0.02	0.79±0.06	0.79±0.06
	Posterior	0.89±0.03	0.78±0.06	0.78±0.06
Perfusion map	Anterior	0.92±0.02	0.84±0.03	0.85±0.04
	Middle	0.88±0.01	0.79±0.06	0.79±0.05
	Posterior	0.87±0.02	0.77±0.07	0.77±0.05

Table S6 Structural similarity index of Fractional ventilation and Spectral analysis from FB

Maps	Slice	M1	M2	M3
Fractional ventilation *vs.* spectral analysis	Anterior	0.88±0.03	0.88±0.03	0.88±0.03
	Middle	0.82±0.02	0.83±0.02	0.81±0.02
	Posterior	0.81±0.03	0.81±0.03	0.79±0.04

https://dx.doi.org/10.21037/qims-22-92